Fuel 332 (2023) 126061

Contents lists available at ScienceDirect

Fuel

journal homepage: www.elsevier.com/locate/fuel

Full length article

Flow loop study of a cold and cohesive slurry. Pressure drop and formation of plugs

Pavel G. Struchalin [a,*], Vegar H. Øye [b], Pawel Kosinski [b], Alex C. Hoffmann [b], Boris V. Balakin [a]

[a] Department of Mechanical and Marine Engineering, Western Norway University of Applied Sciences, Inndalsveien 28, Bergen, 5063, Norway
[b] Department of Physics and Technology, University of Bergen, Allegaten 55, Bergen, 5007, Norway

ARTICLE INFO

Keywords:
Multiphase flow
Plug formation
Ice slurry
Pressure drop
Rheology

ABSTRACT

Slurries of cohesive particles constitute a significant risk during subsea petroleum production due to their potential to plug the flow. This article describes a flow loop study of a slurry consistent with 0.23-mm ice particles in decane. The experiments were conducted for the concentration of particles up to 20.3% vol. and Re < 25000. The cohesion of ice was suggested by controlling the temperature of the slurry. The relative viscosity of the slurry was computed as a function of particle concentration using pressure drop measurements. The relative viscosity was 3.1 for the concentration of 20.3%. The Bingham-fluid model agreed with the empirical calculations within the discrepancy of 15.5%. Increased viscosity of slurry led to a higher pressure drop in the flow loop compared to the single-phase case. Pressure drops for 20.3% slurry flow were 5.2% and 44.4% higher than for pure decane at Reynolds numbers of 24778 and 4956, respectively. The test section of the loop was equipped with an orifice to induce the formation of plugs. The plugs were observed at particle concentrations below 7.0%. The article presents detailed experimental logs depicting the process of plug formation. The observed blocking cases partially agreed with flow maps from the literature. In addition, we note the applicability of the blockage risk evaluation technique from the Colorado School of Mines.

1. Introduction

Slurry flows are frequent in energy technology. One of many examples is coal slurries, which are used for a low-cost transport of fine coal particles and efficient coal combustion [1]. Also, slurries occur as drilling muds in the petroleum industry [1] and as coolants in refrigeration processes [2]. Generally, pipe transport of slurries is a challenging problem. The particle size often varies between tens to hundreds of microns, and such particles settle under gravity without sufficient flow agitation. Particulate deposits are thus formed in stagnation zones often associated with local flow restrictions.

The issue of deposit formation is crucial in petroleum flow assurance. Deposits of solid particles increase pumping costs and negatively alter the flow morphology. In this context, the most problematic slurries are those containing cohesive particles, i.e., gas hydrates, wax, and their mixtures [3–5]. In addition to the formation of deposits, the cohesive particles may plug the whole pipeline cross-section. There are many detailed experimental studies of hydrate slurries. Majid et al. [6] considered the formation and flow of a methane slurry in a 4-inch flow loop filled with a three-phase mixture of crude oil, brine, and methane. Their research revealed significantly elevated pressure drops if more than 15% of hydrates were formed in the slurry, mainly if the oil content was high. It means the cohesion between hydrate particles is weaker in water-dominated systems. A similar result was obtained by Vijayamohan et al. [7] for a natural gas hydrate slurry in a 3-inch flow loop. None of these works studied the process of plugging in detail, as those papers dealt with complex high-pressure systems where multiple parameters of the slurry were uncertain. These parameters were the particle size, cohesive force, and volume fraction of the particles.

To ease the experimental characterization of the slurry, it is possible to combine the desired parameters of the flow into the apparent viscosity and yield stress. There are various works where flow loop pressure measurements are interpreted in terms of the rheology of hydrate slurries. Darbouret et al. [2] conducted laminar flow loop experiments using a water-based slurry of tetra-n-butylammonium bromide hydrate. The authors found that the slurry was a Bingham-type fluid with yield stress up to 4 Pa at 50% particle load. Fidel-Dufour et al. [8] studied a laminar slurry of methane hydrates that were formed in a water-dodecane emulsion. They found that the slurry's apparent viscosity depends on the particle's mean size and that the relative viscosity of the slurry is above 6.0 at the particle concentration of 16%. The rheological expression by Snabre and Mills [9] was used by Fidel-Dufour et al. [8] to fit the experimental data. In addition, it is

* Corresponding author.
E-mail address: pstr@hvl.no (P.G. Struchalin).

https://doi.org/10.1016/j.fuel.2022.126061
Received 4 May 2022; Received in revised form 26 August 2022; Accepted 17 September 2022
Available online 11 October 2022

challenging to relate the obtained rheological studies to an industrial case that is supposed to be in a turbulent regime. A comprehensive rheological study of a natural gas hydrate slurry was recently conducted by Ding et al. [10]. The analysis was performed in a 25-mm flow loop for an emulsion-hydrate slurry, controlling the pressure drop and the particle size in the system. They found that the rheological expression by Snabre and Mills [9] fitted the experimental results well and that a significant amount of unconverted water was trapped inside hydrate shells. Therefore, hydrate-based slurries may be characterized by an effective volume fraction beyond the actual solid content in the system. The flow parameter is the effective volume fraction, which is uncertain for a realistic industrial system. Despite the greater certainty in the design of the rheological experiments, there was no plugging formation reported there [2,10]. This is most possibly since a rheological analysis requires a homogeneous flow in the system. However, the process of plugging is also dependent on the local flow parameters and geometry of the process.

Ice slurries may contribute to a more accurate design of flow-assurance experiments as ice particles constitute a suitable model of gas hydrates. In this case, the concentration and the initial size of the particles may be controlled by precisely dozing the ice directly into the slurry. The thermal stability interval is similar for a majority of hydrates [3] and the cohesion of the ice is also similar to that of hydrates and is well known for different conditions [11,12]. There is a significant knowledge base on experiments with the ice slurries used in refrigeration [13]. In these studies, the concentration of the particles was up to 40% [14,15], and the size of the particles was typically under 1.0 mm [16,17].

Niezgoda-Żelasko and Żelasko [15] measured the pressure drop in a flow loop with slurries with 100~150 μm particles at concentrations under 30%. They found that the pressure drop significantly increased with ice concentration for laminar and transitional flow regimes. However, the particle presence did not contribute to the pressure drop in the turbulent flow regime. Moreover, the pressure drop in the slurry was lower than that in the one-phase flow of the pure carrier fluid for the same flow velocity.

Onokoko et al. [18] analyzed pressure drop in a pipe flow of slurry loaded with up to 20% wt. ice particles. A slight influence of the particle concentration on the pressure drop was noted for flow velocities above 2 m/s. However, in [15], a doubling of pressure drop decrease was detected at 0.08 m/s when the ice concentration was increased from 5% wt. to 20% wt.

Rayhan and Rizal [19] studied water-based ice slurry with methanol in the flow loop. They found that Doetsch and Christensen models could not adequately predict the pressure drop in slurries, obtaining a four-fold increase in the laminar regime at a particle concentration of x = 29% wt. They proposed a new model and noted that slurries showed both Newtonian ($3\% < x < 5\%$ wt.) and pseudoplastic behavior ($x > 9\%$ wt.).

Bordet et al. [14] considered the pressure drop and flow patterns in a straight horizontal pipe with an ice slurry laden with 250 μm particles at concentrations up to 18.4%. The experiments showed that the pressure drop was 1.6 times higher for 18.4% ice slurry than for the pure carrier fluid at 0.6 m/s, and the slurry pressure drop was 21.7 times higher than that for pure fluid at 0.025 m/s. A majority of the reported flow experiments with ice slurries in the literature did not result in plugging of the pipe [13]. This is probably due to the fact that the carrier fluid involved was an aqueous solution of ~10% ethanol or glycol, whose presence decreases the cohesion of ice.

There are a few experimental studies of *cohesive* ice slurries for petroleum flow assurance. Rensing et al. [20] conducted experiments on an ice slurry in crude oil at ice concentrations up to 70%. The slurry was produced by cooling a water-in-oil emulsion with a droplet size below 3 μm. During the experiments, it was found that the slurry was shear-thinning for concentrations above 10%. The relative viscosity of the slurry was equal to 25 at the concentration of 50%. There was yield stress detected in the slurry at concentrations above 25%. The yield stress was in the interval of 300 to 3000 Pa. The relative viscosity of the slurry produced from a brine-in-oil emulsion was at least twice lower than for a pure-water–ice slurry. This indicated a higher cohesion for the latter case.

The work by Hirochi et al. [21] is among but a few experiments on plugging in ice slurries. In this work, an experimental system consisting of a 52-mm pipeline was blocked by a water–ice slurry. The plugging was induced by an orifice inserted into the pipe. The particle size was 1 mm, and the concentration of the particles was up to 40%. A flow map of the plug formation was determined in the experiments. According to the flow map, a plug was formed in a very dilute slurry at a flow velocity lower than 0.12 m/s, while blockage was impossible at 0.5 m/s until the concentration increased beyond 32%.

In our research, we further developed the experimental approach proposed by Hirochi et al. [21]. For this, we conducted a series of flow loop experiments using a decane-oil slurry. The loop was also equipped with an orifice to localize the place where the plug can be formed. We investigated the potential location and rationale for how plugs are formed in the system. In our tests, we accurately controlled the concentration and size of the particles. In addition, by exploiting micro-mechanical measurements by Yang et al. [12], we set the temperature of the flow to control the cohesion between the particles. This paper provides a precise definition of flow geometry and experimental conditions. Together with the detailed information on the formation of particulate obstructions in the loop, they formulate a suitable benchmark for validating numerical models of plugging.

2. Experiments

2.1. Ice slurry

The ice slurry used in this study was made from decane (liquid phase) and ice particles (solid phase). Decane with a chemical purity of >99% was supplied by Sigma Aldrich company, while the ice was produced in-house from tap water. The typical chemical composition of the water is presented in Supplementary materials (Bergen Vann, annual water quality report). Surfactants were not used in the experiments.

For the tests, ice slurry was prepared through several stages. First, the required mass of ice was produced as ice cubes in a freezer at −22 °C. Then, the ice cubes were crushed and mixed with a small amount of decane in a blender (BN750EU from Ninja).

The resulting ice particles were investigated by means of optical granulometry. Pictures were taken by a Leica Quad Camera (20 MP, f/2.2, 16 mm). We analyzed the photos of the particles taken from the samples of freshly produced slush before they were charged into the flow loop. We also took samples from the flow loop during the experiments.

The obtained photos were treated in the Image-J software with the standard functions “Analyze” and “Analyze particles”. The treatment aimed to determine the boundaries of particles and estimate the particle size as the diameter of a sphere with an equivalent projected area.

The produced concentrated slush was cooled down to −22~−25 °C and stored in a freezer. The pure decane was kept at the same temperature. At the test start, the decane and required slush mass were poured into the expansion tank (see Fig. 1) and stirred there.

2.2. Flow loop

The experimental set-up is depicted schematically in Fig. 1. A closed flow loop where ice slurry was pumped through a transparent test section. The test section was a straight horizontal pipe, 1.73 m in length, 22-mm inner diameter, and a 1.5-mm wall thickness. The walls of the tubing were made of 304 stainless steel. A blind-T flow restriction conditioned the flow profile at the entrance to the test section. The section was equipped with an orifice to increase the probability of plug

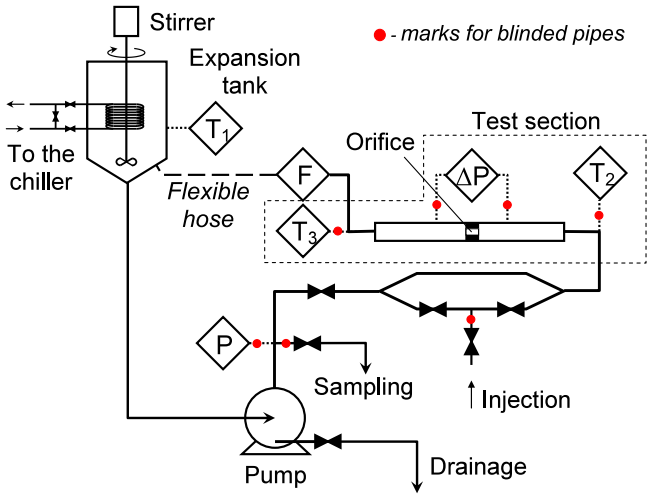

Fig. 1. The hydraulic scheme of the flow loop. P, T, F denote pressure, temperature, and flow rate measurements.

Table 1
Measurement system.

Parameter	Sensor	Meas. range	Inst. error
Temperature	PT100 + LKM 103 Transducer	−40~85 °C	±0.1 °C
Pressure	Gems 3500 Pressure Transmitter	0~4 bar	0.25%
Differential pressure	Omega PXM219-006AI	0~6 bar	0.25%
Flow rate	Micro Motion Coriolis Flow Meter (R050S Sensor,1700 Transmitter)	0~3600 kg/h	0.5%

formation. The diameter of this restriction was 9.5 mm, and the length was 10 mm. Also, there were two facets (1 mm × 45°) in the orifice.

The orifice was installed at a distance of 85 cm from the test section inlet. It corresponds to 38.6 hydraulic diameters. The orifice was mounted inside a 110-mm transparent glass pipe (borosilicate glass 3.3). The test section was connected to the rest of the loop using two 90-degree T-junctions. The total length of the steel pipes in the loop was 6.7 m. There were also 1.3 m of flexible hoses that enabled changing tilt angles of the test section. The internal surface of the hoses was covered with smooth nitrile rubber. The loop included two 45° bends in the metal pipes after the pump and fourteen 90° bends in the pipes in total (including the turns inside the flowmeter). A bifurcation of the pipes between the pump and the test section included an injection port.

For pumping the slurry, we used a centrifugal pump (Pedrollo HF 70 A, 2.2 kW) coupled with a frequency converter (ABB ACS355). We altered the flow rate in the system using the frequency converter. The casing of the pump was made of cast iron, and the closed-type impeller was made of brass. The axial clearance in the pump was 4 mm. The impeller with seven blades had a thickness of 10 mm and a diameter of 200 mm.

The measurement system of the flow loop consisted of a digital manometer at the outlet from the pump, a differential manometer at the test section, a Coriolis mass flowmeter after the test section, and several sensors for temperature control. The internal geometry of channels in the flow meter was clarified by means of supplementary computer tomography. The specifications of the sensors are presented in Table 1. The sensor signals were collected and processed using the National Instrument 6001 DAQ USB data card operated under a LabView-based control program with an acquisition frequency of 1 kHz.

The flow loop included an expansion tank made of 304 stainless steel and open to the atmosphere. The tank was used for filling, cooling, and dispersion of the slurry. The tank consisted of a cylindrical top part (⌀310 mm, 310 mm height) and a conical bottom part (⌀35 mm bottom, 230 mm height). The total volume of the tank was 29.9 l. A coil heat exchanger was installed inside the tank and connected to the chiller (WTG-Quantor Chilly 25 M-LT). The heat exchanger was built of SS 304 metal pipe (⌀10 × 1 mm) and had fourteen coils of a rounded rectangular shape with the sides of 120 × 50 mm and a radius of 25 mm. The cooling system had a bypass line for changing the flow rate of the coolant. Using a bypass line of the heat exchanger, we set the temperature in the tank with the accuracy of ±0.2°C relative to the required temperature. The coolant was a 35% vol. propylene glycol–water mixture. The coolant was pumped by Y 2051.0263 pump delivering 0.44 m^3/h at 3.0 bar.

An overhead stirrer (Joanlab OSC-20L) with a 75-mm three-blade impeller continuously operated at 1700 rpm and homogenized the slurry during the tests. Two layers of polyethylene foam thermally insulated the outer surfaces of the loop. The average thermal resistance of the walls was 5.3 (m^2·K)/W. The set-up was placed in a room that was controlled by an automatic energy management system. The room temperature was within the range 21.2~25.4 °C.

The tests were performed following an established procedure. First, the chiller was set to −9 °C. Thereafter, the pre-cooled pure decane was charged into the loop, and the pump was started at 1600 kg/h. The pre-cooled pure decane cooled down the loop elements to negative temperatures, which prevented the initial melting of the ice particles. Next, the stirrer was activated, the flow was increased up to 2200 kg/h, and the concentrated ice slush was loaded to the tank. In case there was no immediate plug formation in the loop, the set-up and the resulting ice slurry were stabilized thermally at −1 °C using the valves in the cooling loop. This temperature was chosen as the lowest subcooling we could maintain for a long time in the rig and so achieve the highest possible cohesion between the particles [12]. Afterward, the flow rate was reduced to 2000 kg/h. The pressure drop measurements started after the pressure and the flow rate fluctuations remained within ±3% of the average value, so the flow was considered in a steady state. We limited the duration of pressure drop measurements to avoid the formation of significant deposits in the loop due to the slurry deposition. During each measurement, the flow was held constant for about three residence times of the system, and then the flow rate was reduced in seven stages down to 400 kg/h. The flow regime remained turbulent, so the particles were agitated due to the turbulent dispersion. Additional visual observation of the flow in the glass pipe indicated that no deposition or bed formation was observed during the pressure drop measurement. Thus, we assume no significant deposit was in the pipes, and the pipe cross-section remained unchanged. This assumption was used for the calculation of slurry viscosity described in Section 3.3. In addition to the pressure drop measurement, we conducted a long-term test to study the deposition of the particles. In this case, we set a constant pump frequency and recorded the flow rate and pressure drop for a long time until a plug was formed. After the experiments, we stopped the flow and cooling and left the slurry for melting. In the end, the set-up was drained, and the separation of decane from the water was carried out by the fractional freezing method. The purified decane was weighed and replenished if necessary.

2.3. Rheological analysis

The dependence of the slurry viscosity, μ_{mix}, on the volume particle concentration, ϕ, was one of the issues studied in this paper. Our research tested various viscosity models of suspensions against the flow loop measurements. Table 2 presents the rheological expressions we used. The analysis was carried out by computing the apparent viscosity of the slurry from the pressure drop measurements. This procedure is described in Section 3.3. Here and further for describing our results, we use *volume* particle concentration.

Table 2
Rheological expressions.

Reference	Expression
Thomas (1965) [22]	$\mu_{mix} = \mu_l \cdot [1 + 2.5 \cdot \phi + 10.05 \cdot \phi^2 + 0.00273 \cdot exp(16.6 \cdot \phi)]$
Snabre and Mills (1993) [9]	$\mu_{mix} = \mu_l \cdot (1 - \phi) \cdot \left(1 - \phi/\phi_{\max}\right)^{-2}$
Brinkman (1947) [23]	$\mu_{mix} = \mu_l \cdot (1 - \phi)^{-2.5}$
Ford et al. (2006) [24]	$\mu_{mix} = \begin{cases} \mu_a + \tau_y/\gamma & \gamma > \gamma_0 \\ \mu_\infty & \gamma \leqslant \gamma_0 \end{cases}$

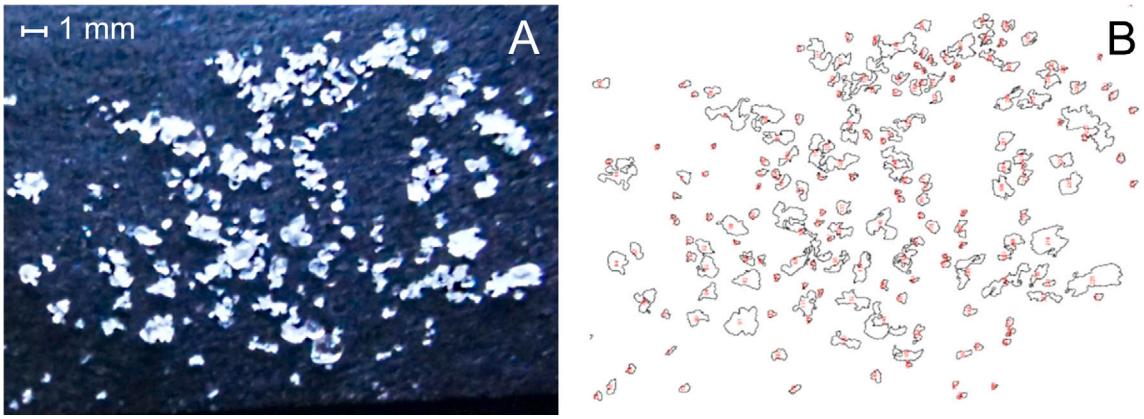

Fig. 2. Ice particles (A) and their contours in Image-J (B).

In Table 2, μ_l is viscosity of the carrier liquid, ϕ_{max} is the packing limit of the particles, τ_y is the yield stress, γ is the shear rate, μ_∞=80 Pa · s [24,25] and $\gamma_0 = \tau_y/(\mu_\infty - \mu_{mix})$ are the limiting viscosity and shear rate, μ_a is the apparent viscosity of the slurry from Thomas' model. We calculated the packing limit ϕ_{max} using the empirical expression by Hoffmann and Finkers [26] for the voidage of a loosely packed bed of the particles ε_{lp}:

$$\phi_{\max} = 1 - \varepsilon_{lp} = (1 - [(1 - 0.416) \cdot \exp(-0.0142\rho d) + \\ +0.416] \cdot \exp(-0.829\sigma)) \cdot \psi^{0.862} \quad (1)$$

where ψ is the mean circularity of the ice particles, σ is the geometrical standard deviation of the particle size distribution, d is the volume mean particle diameter in μm, and ρ is the particle density relative to the density of water.

The yield stress in Bingham's model (taken from Ford et al. [24]) is given as [27]:

$$\tau_y = \sigma_s \cdot \left(\frac{2}{5\pi}\right) \cdot \left(\frac{\phi}{\phi_{\max}}\right)^{\frac{3}{3-fr}}, \quad (2)$$

where fr is the fractal dimension of particles. In Eq. (2), $\sigma_s = F_c/d_0^2$ is the strength of a bond between the particles of size d_0 [27]. The cohesive force for the ice particles in decane F_c was taken from the micromechanical measurements presented in Yang et al. [12]. For this purpose, we approximated the experimental dataset from [12] by a polynomial using function *numpy.poly1d* in Python 3.8 [28]. We computed the cohesive force using the polynomial for the cases within the experimental temperature interval [12]. The shear rate γ was computed using a system of equations for isotropic turbulence in a pipe flow [29].

3. Results and discussion

3.1. Ice particles

Fig. 2 presents a characteristic appearance of the ice particles in a fresh slurry. It is clear that the ice particles are of a fractal-like, irregular shape: they have rough surfaces with perceptible protrusions. The shape of the particles is defined by the size of the primary ice crystals and the mechanics of the ice crushing process.

The particle size range is between 0.2 to 2.1 mm (Fig. 3A). The particle size distribution (PSD) has a single mode at 0.41 mm, and a standard deviation of 0.39 mm. The average circularity of the particle projections to the focal plane of the camera is 0.525. Here and further, all the PSD are well described by the log-normal distribution curve.

Based on analysis of 14 data samples and using the method from [30], an average fractal dimension of the particles was estimated as 2.57. According to Eq. (1), the packing limit of the ice powder was ϕ_{max} = 0.56. This value was close to the one reported by Hirochi et al. [21] for an ice–water slurry.

Fig. 3B illustrates the particles taken from slurry flow at 2000 kg/h. The sample was taken after the thermal stabilization of the flow, directly before the pressure drop measurement. The in-situ morphology of the particles is similar, resulting in a single mode of the PSD at 0.23 mm and a standard deviation of 0.48 mm. The circularity of particles from the sample is 0.482. Analysis of 28 samples of slurry taken at different flow rates and particle concentration showed some variation in average size of the particles (±0.1 mm) and circularity (±0.2).

From the sampling results, we concluded that there was no significant agglomeration of particles. A smaller particle size could be explained by partial melting in regions where the particles could collide with the walls where the local temperature was positive, most likely in the pump. Another reason could be the sampling procedure itself, as the sampling velocity was lower than the mean flow velocity in the loop, and the sample was taken through a branch of a T-junction. Therefore, the largest particles could deposit before they left the system.

3.2. Pressure drop

The pressure drop (PD) was measured for the slurries with volume fraction up to 20.3% both at the orifice and over the entire loop (between the "P" sensor point and expansion tank inlet).

As expected, the pressure drop rises in the slurries with an increase in the flow rate following the dependence of a power-law type (see Fig. 4). In Fig. 4 we present the pressure drop in slurries of various particle concentration, ΔP_s, and decane, ΔP_d, between pump outlet and expansion tank, as well as their relative pressure drops $\Delta P_r = \Delta P_s/\Delta P_d$.

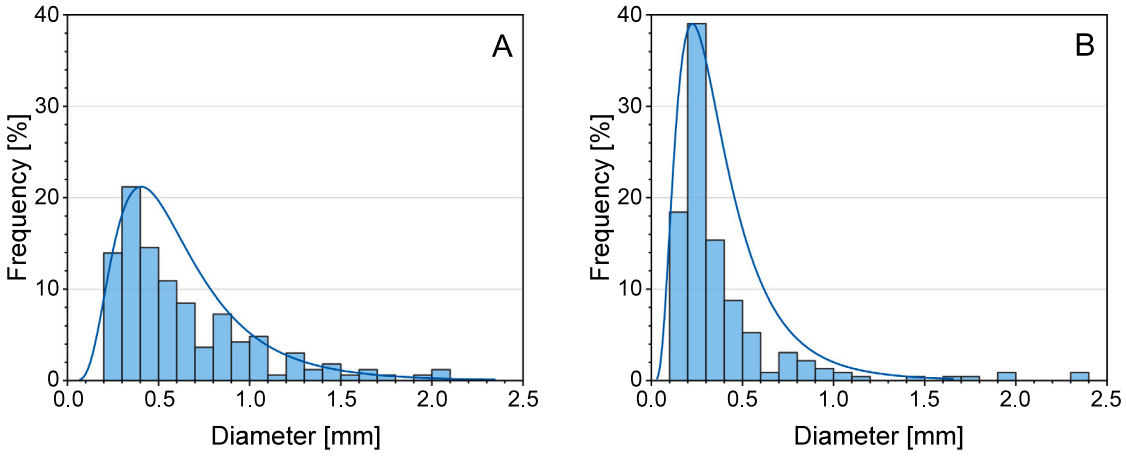

Fig. 3. Particle size distribution in fresh slurry (A) and an *in-situ* sample (B).

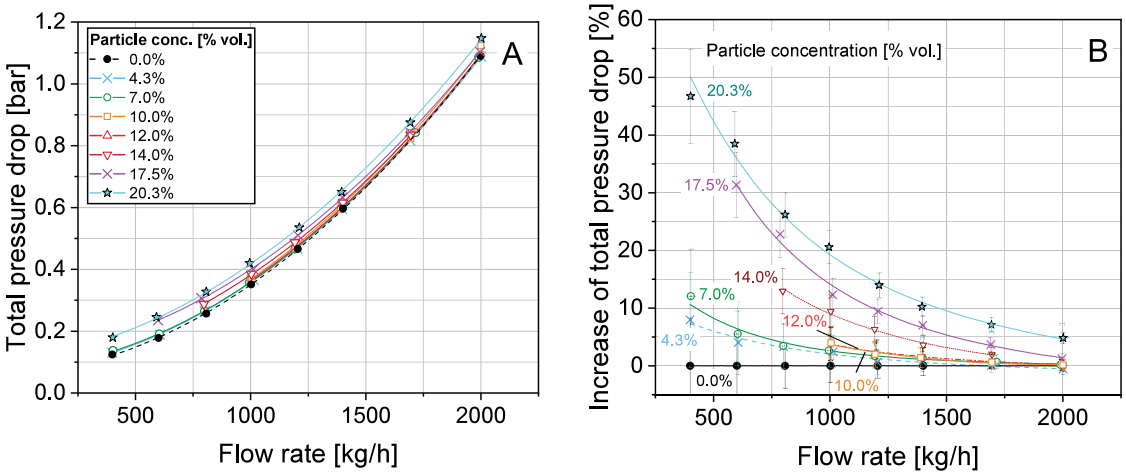

Fig. 4. Absolute (A) and normalized (B) total pressure drop in the ice slurry flow (between "P" pressure sensor and the expansion tank).

Here, we see, the pressure drop varies differently when the particle concentration increases. For example, at the minimum flow rate (400 kg/h, Re = 4956), the pressure drop over the section containing the orifice was 0.010 bar for pure decane and 0.015 bar for 20.3% slurry (50% higher), while at the maximum flow rate (2000 kg/h, Re = 24778) the values were 0.330 bar for pure decane and 0.331 bar for 20.3% slurry (0.3% higher). Similar results were obtained for the PD across the loop, where the PD at 400 kg/h was 0.124 bar and 0.179 bar in pure decane and 20.3% slurry (44.4% higher); and 1.09 bar vs. 1.147 bar (5.2% higher) at 2000 kg/h.

The obtained results are consistent with the previous studies of ice slurries based on aqueous solutions of alcohols. Niezgoda-Źelasko and Źelasko [15], Onokoko et al. [18], Bordet et al. [14], and Illan and Viedma [31] observed that the PD increased at a reduced flow velocity yet an increased particle concentration.

Considering the concentration of the particles in the slurry, we classify the flow as collision-dominated [32]. The effect of the particle concentration on the pressure drop in the slurry flow is due to an enhanced energy dissipation caused by inter-particle and particle–wall interactions.

It should also be noted that particle deposits appear on the inner surfaces of the pipes over time. The flow conditions influence the size and structure of the deposits. The lower the flow rate, the larger the deposits are. This attributes to the significant PD increase with the concentration of the flow rates under 1000 kg/h.

3.3. Flow rheology

The relative velocity of the slurry was obtained from the pressure measurement. For this, we assumed a homogeneous slurry flow for the entire interval of the considered flow rates. Then the PD between the pump point ('P') and the expansion tank was computed from:

$$\Delta p = \sum_{i=1}^{N} \lambda_i \frac{l_i}{d_i} \frac{\rho_{mix} u_i^2}{2} + \sum_{j=1}^{M} \xi_i \frac{\rho_{mix} u_j^2}{2} + \rho_{mix} g z_p, \tag{3}$$

where l_i and d_i are the length and the equivalent hydraulic diameter of ith pipe element on the way to the tank; u_i and u_j are the average flow velocities in the pipe element and in the jth local flow restriction (e.g., bend, orifice). Furthermore, $\rho_{mix} = \phi_p \rho_p + \rho_l (1 - \phi_p)$ is the density of the mixture with the volume fraction of particles ϕ_p with indices denoting the particles (p) and the carrier liquid (l). The hydrostatic pressure difference is defined by the elevation of the tank z. The friction coefficients λ_i and the local flow resistance coefficients ξ_i were set dependent on the local Reynolds number Re_i. We calculated these coefficients following Idelchik [33]. A complete set of the used equations is available in the Supplementary Materials.

Based on pressure drop measurements, we estimated the viscosity of the slurry using Eq. (3). For this, the pressure drops over the entire loop were calculated within the range of experimental flow rates for each particle concentration with a variable value of slurry relative viscosity. Then, using the least squares method, we found the slurry apparent viscosity that provided the best agreement between the calculated and

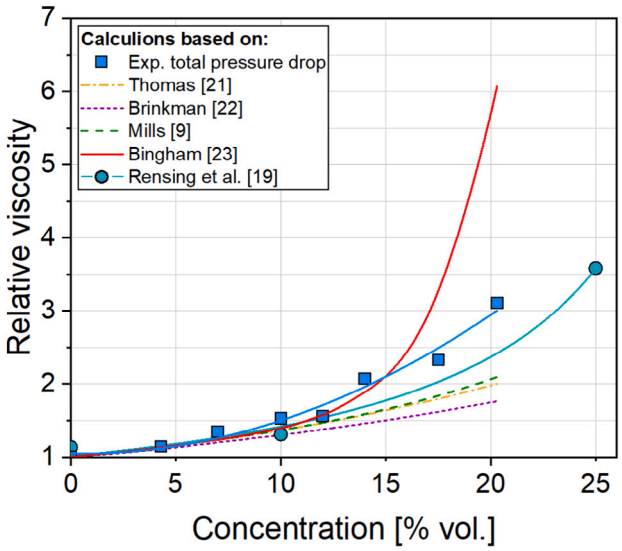

Fig. 5. Relative viscosity of ice slurry.

experimental pressure drops for the entire range of the considered flow rates. the local Reynolds number was computed from $Re_{i/j} = \rho_{mix} u_{i/j} d_{i/j} / \mu_{mix}$.

The results of the calculation are presented in Fig. 5 in terms of the relative viscosity μ_{mix}/μ_l for different particle concentrations. In this figure, the results for Bingham's model are averaged over the experimental interval of flow rate variation. The figure demonstrates that the relative viscosity rises with the particle concentration, achieving the value of 3.1 at 20.3% concentration. It should be noted that a more detailed rheological study of the slurry could show variation in viscosity at different shear or flow rates. This is indirectly confirmed by a rising pressure drop in slurry flow with a reduction in flow rate (Fig. 4B).

Two primary reasons explain this phenomenon: enhanced dissipative interactions in the particulate phase and the momentum coupling between the particles and fluid.

To verify the validity of the applied rheological approach, in Fig. 5 we also present experimental results from Rensing et al. [20] for a similar oil-based slurry of ice. We see that the relative viscosity is up to 21.9% lower. This is explained by our experiments being carried out at a lower subcooling of –1 °C. This resulted in stronger cohesion between the particles.

From Fig. 5, we conclude that the models of Brinkman, Thomas, and Mills give comparable calculated values of the relative viscosity. They agree with our experimental data up to 12% of particle concentration. The average discrepancies at $\phi < 12\%$ for Brinkman, Thomas, and Mills models are 10.3%, 6.9%, 6.5%, respectively, and the maximum discrepancies are 14.8%, 10.7% and 10.5%. However, a higher mismatch between these models and our data appears for denser slurries ($\phi >$ 12%), leading to discrepancies up to 43.2% (Brinkman). At the same time, the data from the Brinkman, Thomas, and Mills models do not show a similar trend. Most probably, the considered rheological models are not applicable for the dense slurry as the flow morphology deviates from homogeneous in this condition.

Treating the slurry as a Bingham fluid yields comparable results to the other models up to $\phi = 15\%$. Increasing particle concentration above this level leads to the rapid growth of the relative viscosity calculated by the Bingham-fluid model. As a result, the computed values reproduce the experimental trend better, with average and maximum discrepancies of 15.5% and 48.8%. Nevertheless, this model is susceptible to the packing limit. This parameter is also the least certain in a dynamic flow condition.

3.4. Formation of plugs

Another study objective was to achieve a controlled plugging of the flow loop. We purposely located the orifice within the test section to do so, thus introducing the most significant local flow restriction. The literature data shows that plugging in cohesive slurries often occurs where the pipe is partially obstructed.

During the tests, we registered several cases when the orifice was blocked. The experimental logs of these cases are presented in Fig. 6 in terms of the temporal variation of mass flow rate at different particle concentrations. In addition, the figure depicts two cases where the flow loop was plugged at another place of the loop. To highlight the differences between the cases, we describe the process of plugging below.

№1. The initial flow rate was 1500 kg/h, and the concentration of the particles was 2.2%. The first partial blockage of the orifice came 3292 s after the temperature and the flow rate were established. During ~600 s, partial blocking of the loop and the orifice occurred. As a result, the flow rate was reduced to ~1100 kg/h. The growth of the obstruction in the orifice and an associated reduction of the flow rate to 500 kg/h occurred after 3.9 h. The formed deposit was unstable. The deposit was also partially resuspended by the flow after 4.4 h. As a result, the flow rate increased to 600 kg/h. Later on, a sudden blockage of the entire cross-section of the orifice occurred. We consider this case in more details in Figs. 7 and in Fig. 8

№2. The initial flow rate was 400 kg/h, and the concentration of the particles was 6.8%. A blockage occurred in 2 min. In this case, we observed a rapid formation of a large particle deposit (e.g. Fig. 8, №4 (left), area circled in red) that swiftly turned into a plug. Compared to case 1, the initial flow rate was substantially lower, and the particle concentration was much greater. Due to the low flow agitation, gravitational deposition of the particles was dominant in this case. The flow regime was slug-type indicating accumulation of particles upstream at local restrictions. The size of the slugs was comparable to the size of the opening in the orifice.

№3. The initial flow rate was 400 kg/h, and the concentration of the particles was 6.9%. The first sign of the blockage appeared after 580 s. Due to this blockage, the flow rate was reduced to ~300 kg/h, but later it was restored. In about an hour from the start of the experiment, a plug was formed in a period of 178 s. For this case, the deposit in the vicinity of the orifice was smaller than in case №2.

We note that the conditions of this case are similar to case №2, while much slower plugging happened here. This can probably be explained by slightly different local flow conditions upstream, particularly variations in the positions where the slugs are formed. This is indirectly confirmed by the pressure records that showed ~7% higher drop before the orifice.

№4. The initial flow rate was 700 kg/h, and the particle concentration was 7.1%. Thus, this case was similar to case №2. The first partial blockage (blockage of a part of the orifice) of the orifice occurred after 120 s when a massive slug blocked the orifice (similar to Fig. 8, №4 (left)). This plug was porous, so the flow was not stopped but reduced to 280 kg/h. Within 166 s after the flow reduction, the plug in the orifice collected more particles from the flow, which reduced the porosity and finally plugged the flow loop.

№5. The initial flow rate was 500 kg/h, and the particle concentration was 7.2%. Partial blockage of the loop took place in 580 s after the start. The deposition occurred at the bottom of the test section. The flow rate was reduced to 250 kg/h, and the flow loop was blocked within 120 s after this flow reduction. There was no plug formed at the orifice. Therefore, the blockage was possibly due to plugging another conduit with a reduced cross-section somewhere in the loop, maybe in the flow meter. An alternative scenario could be the formation of a massive deposit in the horizontal pipes of the loop. In this latter case,

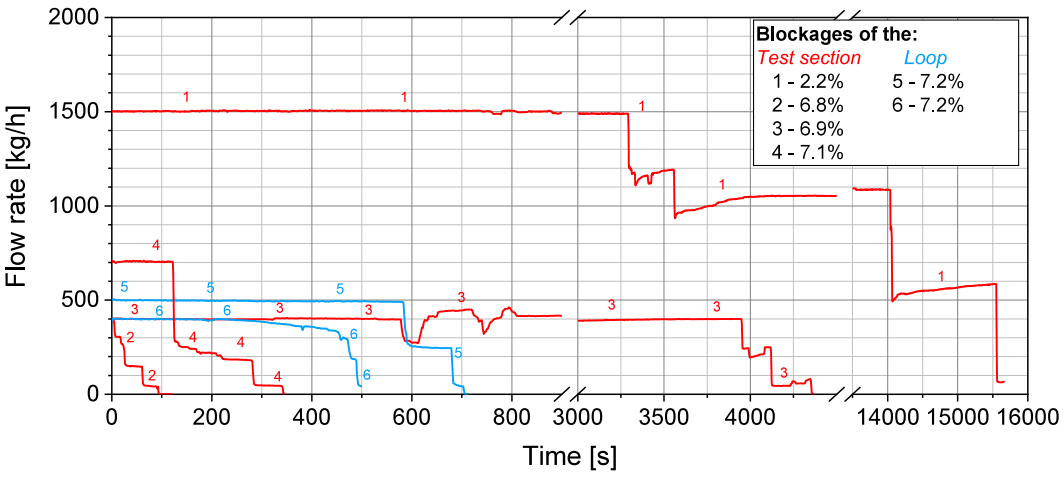

Fig. 6. Experimental logs during plugging.

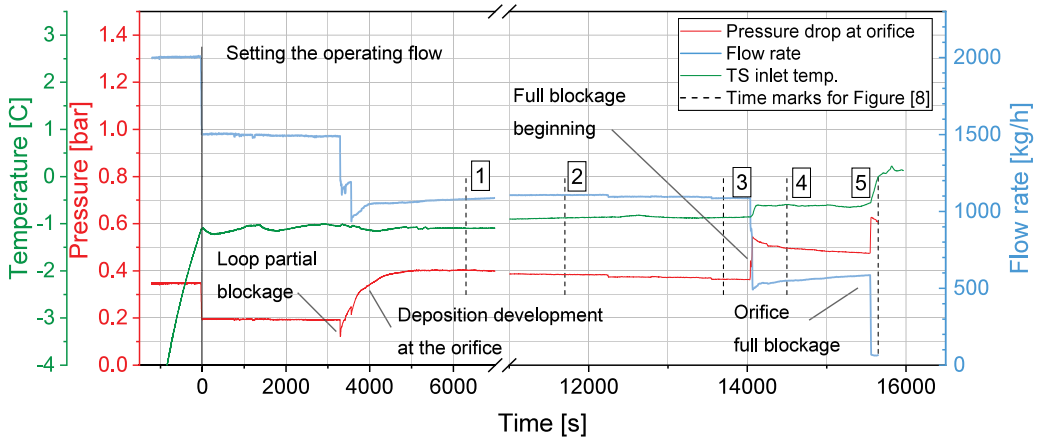

Fig. 7. Experimental log for case №1.

a uniform narrowing of the cross-section raises the flow resistance and dramatically reduces the flow. The blockage time is comparable to cases №2 - 4.

№6. The initial flow rate was 400 kg/h, and the particle concentration was 7.2%. The growth of the deposit at the bottom part of the test section led to a gradual decrease in the flow rate down to 300 kg/h, which happened 470 s after the start. This initiated a rapid blockage of the loop after the test section. Considering cases 2, 3, and 6, with similar experimental conditions, it is seen that plugging happens either at the orifice or in the loop. This means that the probability of plugging is comparable in many regions of the flow loop for low initial flow rates.

In Fig. 7, we provide a detailed experimental log for case №1. This case resulted in the slowest evolution of the plug at a low particle concentration of 2.2%. The set-up and the slurry flow were first stabilized thermally to −1 °C at the inlet to the test section according to the measurement procedure. Then, the flow rate for this experiment was set at 1500 kg/h. For the next 3200 s, the flow rate remained stable. The pressure drop was constant at 0.2 bar. After about 3290 s, the flow rate fell to 970 kg/h. At the same time, the differential pressure over the test section reduced to ~0.15 bar and then suddenly rose to 0.4 bar. Thus, we concluded that a partial blockage of the loop occurred and then initiated a partial blocking in the test section. Here we think that there were particles accumulated in the blind bends upstream of the test section during the initial period. They were further suspended and next deposited in horizontal pipes as a stationary bed of the particles.

A decrease in the flow rate leads to the beginning of a ring-like deposit formation near the orifice. The deposit was formed at the frontal edges of the orifice and all over the sidewall of the pipe. During the following 10600 s, the growth of this deposit coincided with the development of a stationary bed of particles along the horizontal pipe. This process is schematically presented in Fig. 8. There was no significant increase in the pressure drop during the ring-like deposit formation process. Due to the increased friction in the slurry, the system was heated up by ~0.5°C but remained at temperatures below 0 °C, without melting of particles in the loop, indicating the increased cohesion in the slurry. A reduction of flow velocity leads to heat transfer deterioration at the cooling coils and contributes to the heating of slurry from the ambient.

After this time, the flow in the system dropped down to ~500 kg/h, lasting approximately 25 s. The stationary bed had reached the orifice and merged with the ring-like deposit. During these 25 s, the flow rate decreased, and a partial blockage of the orifice occurred. This led to an increase in the differential pressure over the orifice to 0.5 bar. As a result of the reduced flow agitation, the turbulent dispersion of the particles was reduced, so fewer particles resided close to the upper wall of the pipe. The gravitational deposition started to dominate, and the particulate flow was shifted towards the bottom of the pipe. The temperature increased by another ~ 0.5°C. This contributed to further growth of the deposit at the bottom of the tube. As a result, after 1000 s, the cross-section upstream the orifice and the orifice were blocked completely. The blockage increased the pressure drop to above 0.6 bar within 13 s. The flow in the loop stopped. The temperatures above 0 °C at the test section inlet is addressed to the formation of a deposit near a temperature sensor working as thermal insulation between the

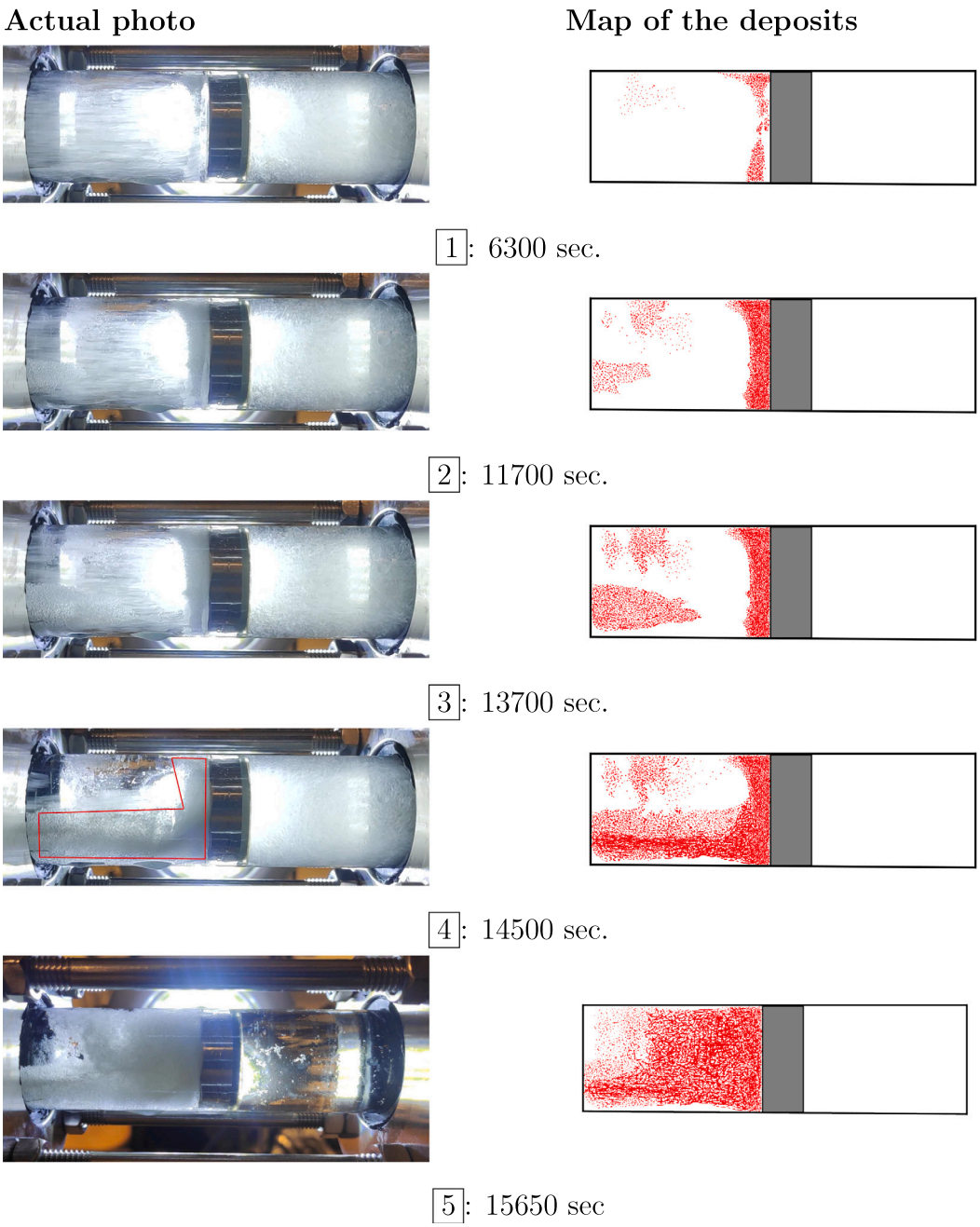

Fig. 8. Schematic description of plugging.

sensor and the main flow. It can happen just before the formation of the plug and does not influence the process of the blockage build-up at the orifice.

3.5. Mapping the plugs

It is interesting to validate the existing methods of plugging prediction against our results. The most traditional approach is based on flow morphology maps. The main parameters governing the morphology of the multiphase flow are the Reynolds number and the concentration of particles [34,35]. Several flow maps are derived from experiments and simulations of systems similar to ours. In Fig. 9, we show how the considered cases appear on the maps presenting the obtained cases of the orifice blocking in the test section. The first map by Poloski et al. [36] is formed by regions of a homogeneous (stable) and a segregated (unstable) flow. The boundaries between these regions derive from the critical particle deposition velocities determined for a particular flow regime. The second is the map of Doron and Barnea [37]. This map indicates the following flow regimes: homogeneous flow, moving bed, stationary bed, and a regime where plug formation is possible. The boundaries between the regimes are obtained from a numerical model. The third map is based on the experimental results by Hirochi et al. [21].

In Fig. 9, we observe deviations between the flow maps and the plugging cases from our experiments. The map of Doron and Barnea [37] predicts the formation of a stationary deposit, while the blockage region is far from our experimental points ($\phi > 0.5$). This is connected to the fact that their model did not account for cohesive interaction and adhesion to walls. According to Poloski et al. [36], initially, our cases were in the stable turbulent flow region without sediment formation. This agrees with the experimental observations, as the flow was homogeneous at the start of the experiment. As in the map by Doron

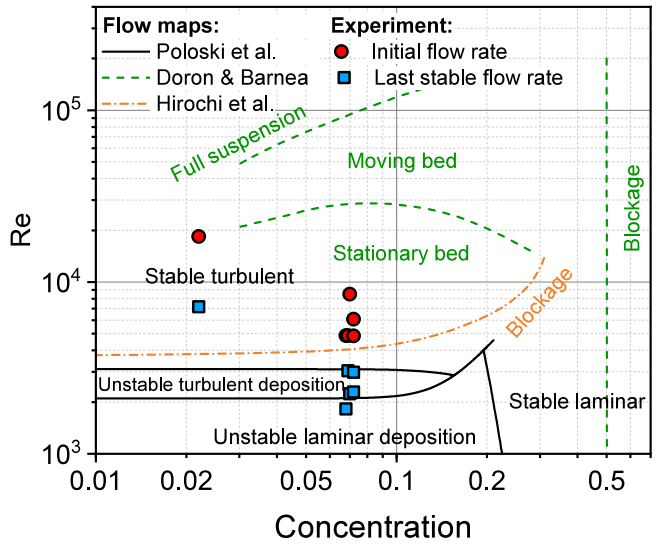

Fig. 9. Experimental results on flow maps from the literature.

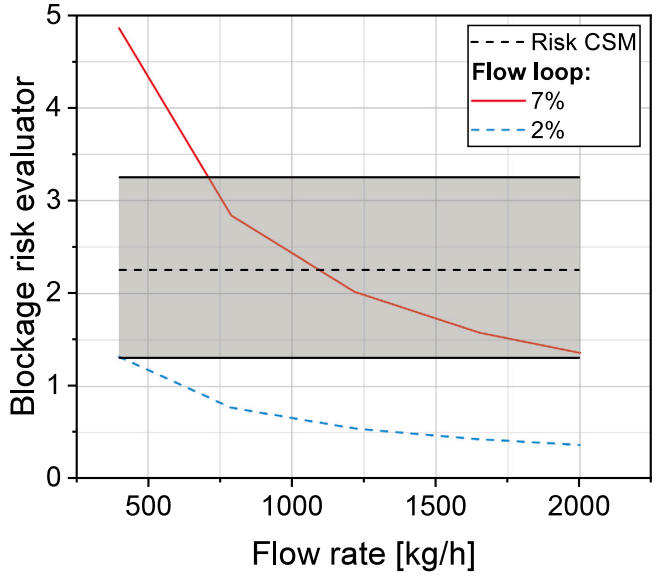

Fig. 10. Blockage risk evaluator.

and Barnea, the flow map by Poloski et al. [36] predicts the formation of deposits when we consider the last stable flow rate. However, this map does not depict the plug formation most possible due to a lower cohesion of the particles used by the authors. A better precision comes from the map by Hirochi et al. [21]. No plugging is predicted for the initially set flow rate, while most of the cases are in the plugging region for the last stable flow rate. We note that this latter flow map comes with the best correspondence to our data as there was a similar orifice in the flow loop used by Hirochi et al. [21]. The open area was 8.3% of the pipe area for the orifice in their work [21]. In our experiments, this ratio was 18.6%.

Another approach to assess the possibility of plugging is the risk-based approach proposed by Chaudhari et al. [38] for a gas-emulsion flow laden with hydrates. The emulsion was formed by water droplets dispersed in an oil phase. Using dimensional analysis and the available statistical data on plugging in a high-pressure flow loop from the Colorado School of Mines (CSM), they proposed an expression for a blockage risk evaluator BRE:

$$BRE_h = 500\frac{\phi/(1-\phi)\,LL}{[Re\,(1-LL)]^{0.52}\,Ca^{0.27}}, \tag{4}$$

where ϕ is the volume fraction of particles, Re is the Reynolds number, LL is the volume fraction of emulsion, and Ca is the capillary number responsible for the solid phase cohesion due to liquid bridges.

There is no liquid other than decane in our ice slurry. Therefore, we adopt Eq. (4). Instead of the standard capillary number, we define a granular capillary number $Ca_g = \mu_l u/\gamma_c$, where u is an average flow velocity, and $\gamma_c = 4F_c/3\pi d_0$ is the interfacial energy per unit area of ice in decane. Fitting the experimental data from Yang et al. [12], we obtain $2F_c/d_0$ ~1.4 N/m for ice in decane at −1 °C. Taking into account that there is no gas in the slurry (LL=1) and making use of the Taylor series expansion, an asymptotic value of the risk evaluator then becomes:

$$BRE = \lim_{LL\to 1} BRE_h = 1042\frac{\phi/(1-\phi)}{Re^{0.52}Ca_g^{0.27}}. \tag{5}$$

In Fig. 10, we present how the BRE depends on the flow rate and concentration of particles. The grey zone in the figure indicates the threshold of BRE_h defined in Chaudhari et al. [38]. Plugging is possible when BRE is greater or equal to the values in the interval.

According to the risk analysis, plugging may occur for the experimental interval of flow rates when 7% of the particles are present in the slurry. This is confirmed by our experiments for cases №2 - 6. However, for case №1 at the concentration of 2%, the risk evaluator indicates that plugging is unlikely, which disagrees with our experimental observation. This case deviates both from the risk-based analysis [38] and from the flow map by Hirochi et al. [21]. The deviation is due to the formation of particulate deposits before the orifice, their partial re-suspension into the flow, and the respective formation of particulate slugs.

4. Conclusion

This paper presents flow loop data for the slurry flow of ice in decane. For this system, the dependence of cohesion on particle subcooling is generally known in the literature. In the experiments, we considered how the pressure drop in the loop depends on the flow rate and the concentration of particles. The volume fraction of particles was below 20.3%, and the Reynolds number was in the range from 5000 to 25000.

During the experiments, we observed that the pressure drop in the slurry was most sensitive to the presence of particles when the Reynolds number was under 10000. Using the pressure drop data, we estimated the apparent viscosity of the flow. Bingham's rheological model correlated the experimental values of the viscosity with the discrepancy of about 15.5%. The computed viscosity was higher than the values predicted by rheological expressions. This is related to the formation of particulate deposits in the flow loop and the respective reduction of the cross-section of the pipe.

In addition to the pressure drop measurements, we identified flow regimes when the particles plugged the flow loop. To achieve plugging, we used an orifice that imposed a significant flow resistance in the loop. Several cases of plugging were studied at particle concentrations of 2.2% and 7%. At the latter concentration, plug formation was often observed within a relatively short running time of several minutes. In the experiments, we observed that large slugs of the ice phase collided with the front surface of the orifice. This initiated a rapid growth of a deposit, blocking the orifice. With a reduction in the particle concentration, the deposit gradually formed near the orifice at a slower speed. The formation of a stationary layer of particles at the bottom of the horizontal pipe was observed, growing in the upstream direction.

We further compared with forecasting of plugging events using flow maps from the literature. The experimental results corresponded well with a flow map developed for a similar system with ice and an orifice. We also adopted a risk evaluation method developed by the Colorado School of Mines. This approach was able to predict plugging.

CRediT authorship contribution statement

Pavel G. Struchalin: Methodology, Investigation, Data curation, Visualization, Writing – original draft. **Vegar H. Øye:** Investigation, Data Curation, Visualization, Writing – original draft. **Pawel Kosinski:** Methodology, Supervision, Writing – review & editing. **Alex C. Hoffmann:** Methodology , Supervision, Formal analysis, Writing – review & editing. **Boris V. Balakin:** Conceptualization, Funding acquisition, Project administration, Supervision, Writing – original draft, Writing – review & editing, Formal analysis.

Declaration of competing interest

The authors declare that they have no known competing financial interests or personal relationships that could have appeared to influence the work reported in this paper.

Data availability

Data will be made available on request.

Acknowledgments

This project was supported by the Research Council of Norway (project 300286). We acknowledge Oleg V. Nikolaev for help with the polynomial fit. P. G. Struchalin tanks Harald Moen, Frode Wessel Jansen, Kjetil Gravelsæter and Nafez Ardestani from Department of Mechanical and Marine Engineering of Western Norway University of Applied Sciences for help in creating the experimental setup.

Appendix A. Supplementary material

Supplementary material related to this article can be found online at https://doi.org/10.1016/j.fuel.2022.126061.

References

[1] Baha Abulnaga P. Slurry systems handbook. McGraw-Hill Education; 2021.
[2] Darboure M, Cournil M, Herri J-M. Rheological study of TBAB hydrate slurries as secondary two-phase refrigerants. Int J Refrig 2005;28(5):663–71. http://dx.doi.org/10.1016/j.ijrefrig.2005.01.002.
[3] Sloan ED. Natural gas hydrates in flow assurance. Gulf Professional Publishing; 2010, http://dx.doi.org/10.1016/C2009-0-62311-4.
[4] Stoner HM, Koh CA. Perspective on the role of particle size measurements in gas hydrate agglomeration predictions. Fuel 2021;304:121385. http://dx.doi.org/10.1016/j.fuel.2021.121385.
[5] Geest Cvd, Melchuna A, Bizarre L, Bannwart AC, Guersoni VC. Critical review on wax deposition in single-phase flow. Fuel 2021;293:120358. http://dx.doi.org/10.1016/j.fuel.2021.120358.
[6] Majid AA, Lee W, Srivastava V, Chen L, Warrier P, Grasso G, et al. Experimental investigation of gas-hydrate formation and particle transportability in fully and partially dispersed multiphase-flow systems using a high-pressure flow loop. SPE J 2018;23(03):937–51. http://dx.doi.org/10.2118/187952-pa.
[7] Vijayamohan P, Majid A, Chaudhari P, Sloan ED, Sum AK, Koh CA, et al. Hydrate modeling & flow loop experiments for water continuous & partially dispersed systems. In: Offshore technology conference. OnePetro; 2014.
[8] Fidel-Dufour A, Gruy F, Herri J-M. Rheology of methane hydrate slurries during their crystallization in a water in dodecane emulsion under flowing. Chem Eng Sci 2006;61(2):505–15. http://dx.doi.org/10.1016/j.ces.2005.07.001.
[9] Snabre P, Mills P. I. Rheology of weakly flocculated suspensions of rigid particles. J Physique 1996;6(12):1811–34. http://dx.doi.org/10.1051/jp3:1996215.
[10] Ding L, Shi B, Liu Y, Song S, Wang W, Wu H, et al. Rheology of natural gas hydrate slurry: Effect of hydrate agglomeration and deposition. Fuel 2019;239:126–37. http://dx.doi.org/10.1016/j.fuel.2018.10.110.
[11] Fan X, Ten P, Clarke C, Bramley A, Zhang Z. Direct measurement of the adhesive force between ice particles by micromanipulation. Powder Technol 2003;131(2–3):105–10. http://dx.doi.org/10.1016/S0032-5910(02)00339-X.
[12] Yang S-o, Kleehammer DM, Huo Z, Sloan ED, Miller KT. Temperature dependence of particle–particle adherence forces in ice and clathrate hydrates. J Colloid Interface Sci 2004;277(2):335–41. http://dx.doi.org/10.1016/j.jcis.2004.04.049.
[13] Kauffeld M, Kawaji M, Egolf PW. Handbook on ice slurries. 359, Paris: International Institute of Refrigeration; 2005.
[14] Bordet A, Poncet S, Poirier M, Galanis N. Flow visualizations and pressure drop measurements of isothermal ice slurry pipe flows. Exp Therm Fluid Sci 2018;99:595–604. http://dx.doi.org/10.1016/j.expthermflusci.2018.04.024.
[15] Beata Niezgoda-Źelasko JŹ. Generalized non-Newtonian flow of ice-slurry. Chem Eng Processi Process Intensif 2007;46:895–904. http://dx.doi.org/10.1016/j.cep.2007.06.008.
[16] Rayhan F, Pamitran A, et al. Effect of ice mass fraction on ice slurry flow for cold energy storage application. Energy Rep 2020;6:790–4. http://dx.doi.org/10.1016/j.egyr.2019.11.159.
[17] Wang J, Wang S, Zhang T, Battaglia F. Mathematical and experimental investigation on pressure drop of heterogeneous ice slurry flow in horizontal pipes. Int J Heat Mass Transfer 2017;108:2381–92. http://dx.doi.org/10.1016/j.ijheatmasstransfer.2017.01.083.
[18] Onokoko L, Poirier M, Galanis N, Poncet S. Experimental and numerical investigation of isothermal ice slurry flow. Int J Therm Sci 2018;126:82–95. http://dx.doi.org/10.1016/j.ijthermalsci.2017.12.017.
[19] Rayhan FA, Rizal R. Pressure drop and non-Newtonian behavior of ice slurry in a horizontal pipe. Int J Heat Mass Transfer 2022;44:200. http://dx.doi.org/10.1007/s40430-022-03503-0.
[20] Rensing PJ, Liberatore MW, Sum AK, Koh CA, Sloan ED. Viscosity and yield stresses of ice slurries formed in water-in-oil emulsions. J Non-Newton Fluid Mech 2011;166(14–15):859–66. http://dx.doi.org/10.1016/j.jnnfm.2011.05.003.
[21] Hirochi T, Yamada S, Shintate T, Shirakashi M. Ice/water slurry blocking phenomenon at a tube orifice. Ann New York Acad Sci 2002;972(1):171–6. http://dx.doi.org/10.1111/j.1749-6632.2002.tb04569.x.
[22] Thomas DG. Transport characteristics of suspension: VIII. A note on the viscosity of Newtonian suspensions of uniform spherical particles. J Colloid Sci 1965;20(3):267–77. http://dx.doi.org/10.1016/0095-8522(65)90016-4.
[23] Pabst W. Fundamental considerations on suspension rheology. CERAM, Silik 2004;48(1):6–13.
[24] Ford C, Ein-Mozaffari F, Bennington C, Taghipour F. Simulation of mixing dynamics in agitated pulp stock chests using CFD. AIChE J 2006;52(10):3562–9. http://dx.doi.org/10.1002/aic.10958.
[25] Pandey G, Linga P, Sangwai JS. High pressure rheology of gas hydrate formed from multiphase systems using modified couette rheometer. Rev Sci Instrum 2017;88(2):025102. http://dx.doi.org/10.1063/1.4974750.
[26] Hoffmann A, Finkers H. A relation for the void fraction of randomly packed particle beds. Powder Technol 1995;82(2):197–203. http://dx.doi.org/10.1016/0032-5910(94)02910-G.
[27] Genovese DB. Shear rheology of hard-sphere, dispersed, and aggregated suspensions, and filler-matrix composites. Adv Colloid Interface Sci 2012;171:1–16. http://dx.doi.org/10.1016/j.cis.2011.12.005.
[28] Python. numpy.poly1d. 2022, https://numpy.org/doc/stable/reference/generated/numpy.poly1d.html, [Online; accessed 31-March-2022].
[29] Flórez-Orrego D, Arias W, López D, Velásquez H. Experimental and CFD study of a single phase cone-shaped helical coiled heat exchanger: an empirical correlation. In: Proceedings of the 25th international conference on efficiency, cost, optimization, simulation and environmental impact of energy systems. 2012, p. 375–94.
[30] Iannaccone P, Khokha M. Fractal geometry in biological systems. CRC Press; 1996.
[31] Illan F, Viedma A. Experimental study on pressure drop and heat transfer in pipelines for brine based ice slurry. Part I: Operational parameters correlations. Int J Refrig 2009;32:1015–23. http://dx.doi.org/10.1016/j.ijrefrig.2008.10.002.
[32] Crowe C, Sommerfeld M, Tsuji Y, et al. Multiphase flows with Droplets and Particles. CRC Press; 1998.
[33] Idelchik IE. Handbook of hydraulic resistance. 4th Edition Revised and Augmented. Begell House, Inc.; 2008.
[34] Peker S, Helvac S. Solid-liquid two phase flow. Elsevier; 2008, http://dx.doi.org/10.1016/B978-0-444-52237-5.X5001-2.
[35] Ramsdell RC, Miedema SA. An overview of flow regimes describing slurry transport. In: Proceedings WODCON XX - Congress and exhibition: The art of dredging. 2013.
[36] Poloski A, Bonebrake M, Casella A, Johnson M, MacFarlan P, Toth J, et al. Deposition velocities of non-Newtonian slurries in pipelines: Complex simulant testing. 2009, PNNL-18316 WTP-RPT-189 Rev. 0.
[37] Doron P, Barnea D. Flow pattern maps for solid-liquid flow in pipes. Int J Multiph Flow 1996;22(2):273–83. http://dx.doi.org/10.1016/0301-9322(95)00071-2.
[38] Chaudhari P, Zerpa LE, Sum AK. A correlation to quantify hydrate plugging risk in oil and gas production pipelines based on hydrate transportability parameters. J Natural Gas Sci Eng 2018;58:152–61. http://dx.doi.org/10.1016/j.jngse.2018.08.008.